Heliyon 9 (2023) e16796

Contents lists available at ScienceDirect

Heliyon

journal homepage: www.cell.com/heliyon

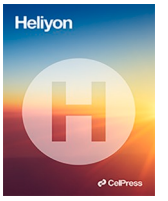

Effect of the relaxation time of mineral oil and monoesters on the fractal dimension and mutual information of creeping discharges propagating along a pressboard

Jean Lambert Jiosseu [a,*], Ghislain Mengata Mengounou [b], Emeric Tchamdjio Nkouetcha [b], Adolphe Moukengue Imano [a,b]

[a] Pure Physique Laboratory UFD MIP, University of Douala, Douala, Cameroon
[b] Laboratory of Technology and Applied Sciences, University of Douala, Douala, Cameroon

ARTICLE INFO

Keywords:
Creeping discharges
Fractal dimension
Mineral oil
Mutual information
Palm kernel oil methyl ester
Relaxation time

ABSTRACT

This paper presents a new method for analysing creeping discharges based on information theory as it applies to medical imaging. The analysis of information surface data is used to determine the impact of relaxation time on the characteristic parameters of creeping discharges. The same information is used to make a comparative study of the morphology of discharges propagating in palm kernel oil methyl ester (PKOME) and in mineral oil (MO). Other comparative methods based on fractal analysis and normality hypothesis tests associated with Anderson Darling (AD), Kolmogorov-Smirnoff (KS) and Shapiro-Wilk (SW) statistics are used. The results show that very short relaxation times increase the error on the measurement of the fractal dimension and the maximum extension of the discharges. A growth of the mutual information between 0 and 60% is observed for relaxation times varying between 60s and 420s respectively. For the same time interval, the *P*-value increases from 0.027 to 0.821 according to the AD statistic, from 0.01 to more than 0.150 according to KS and from 0.083 to more than 0.1 according to SW. This result indicates that the data are from a normal distribution. After 420s of relaxation, the error on the maximum extension measurement is reduced by 94% in PKOME and 92% in MO. Similarly, the error on the mean fractal dimension in MO is reduced by 86.7% for a relaxation time between 301s and 420s, and by 84.6% in PKOME for a time between 180s and 420s. These different results imply that the impact of the discharge can be predicted when it is in its initial phase during which the number of discharge occurrences is reduced. On the other hand, the physicochemical characteristics of the insulating liquid used dictate the relaxation time to be allowed for the laboratory measurements.

1. Introduction

The solid/liquid insulation system is one of the important parts for the survival of high voltage equipment, in this case the power transformer [1,2]. However, it is known that due to the effect of high electrical stresses, the solid/liquid contact points are usually the seat of creeping discharges. This phenomenon contributes to the progressive degradation of the insulation system [3]. Understanding

* Corresponding author.
E-mail address: lambert2008@yahoo.fr (J.L. Jiosseu).

https://doi.org/10.1016/j.heliyon.2023.e16796
Received 1 March 2023; Received in revised form 16 May 2023; Accepted 29 May 2023
Available online 1 June 2023

the process behind these creeping discharges is an important challenge for the preventive maintenance of high voltage equipment.

The analysis of the behaviour of creeping discharges at the solid/liquid interface for the characterisation of insulating liquids is still relevant. Several sophisticated techniques for analysing this phenomenon are common in recent and earlier work. Sitorus et al. [4], rely on the characterization of these discharges through the calculation of the maximum branch extension. This technique allowed them to conclude that Jatropha methyl ester has the same capacity as mineral oil to stop the propagation of creeping discharges. Kebbabi et al. [5] make an experimental characterisation of the phenomenon. In particular, they evaluate the effect of the thickness and nature of the solid insulator on the maximum extension and density of the branches produced. Their work shows that the length of the discharges is clearly reduced for solid insulators with a greater thickness. They also show that the relative permittivity of the solid/liquid insulation system has a significant impact on the occupancy density of the discharges. The same result is observed on the maximum length of the discharges. Beroual et al. [6] study the behaviour of these discharges through a fractal analysis of the phenomenon. The experiment shows that, for a given voltage level, the fractal dimension decreases as the thickness of the solid insulator increases. Similarly, the fractal dimension increases for liquids with reduced permittivity. Reffas et al. [7] evaluate the effect of the electrode system configuration on the extension of discharges in mineral oil compared to vegetable oils. The experimental results show that there is a linear relationship between the maximum lengths of the discharges and the applied voltage. They find that the slopes of the maximum lengths are dominant for vegetable oils compared to mineral oil. The study proposed by Ediriweera et al. [8] consists in evaluating the effect of the shape of the solid insulator on the area occupied by the discharges. They show that, for a given voltage level, solid insulators with a circular shape stop discharges relatively less than a square-shaped insulator. Li et al. [9] observe the inception voltage and charge produced by these discharges under a combined AC and DC voltage stress. The results of the work show that the propagation of creeping discharges is difficult to induce with this voltage combination.

All approaches to discharge analysis proposed in the literature have proven to be very effective in characterising creeping discharges. The new method which is the subject of this work does not discredit the others, but provides additional information on the morphology of discharges. Indeed, the various articles available on the subject of creeping discharges do not highlight the impact of the relaxation time between consecutive lightning strikes on the various parameters observed. This article is devoted on the one hand to the evaluation of the propagation of creeping discharge propagating along a pressboard immersed in insulating liquids. The two liquids being compared are palm kernel oil methyl ester and mineral oil. On the other hand, an analysis is made to evaluate the impact of the relaxation time on the characteristic parameters of creeping discharges. The parameters examined are maximum extension of the discharge and fractal dimension. One part of the study is based on the analysis of the distribution of the sample data by statistical laws. The other part uses a new parameter which is the mutual information based on Shannon's theory.

2. Background on mutual information and hypothesis testing

2.1. About mutual information

Spatial matching of images by robust registration is essential for many clinical tasks. These include image fusion, creation of organ atlases and tumour growth monitoring [10,11]. One of the most widely used methods is based on information theory [12,13]. Indeed, mutual information between two images is the amount of information that one image contains about the other and vice versa [14]. Image registration by mutual information is one of the most widely used techniques, due to its accuracy and robustness [15–17]. In general, the maximum amount of information between images from different sources is reached when they are matched. Registration is therefore an essential step in the image processing chain. The objective of registration is to estimate a geometric transformation allowing the spatial superposition of the structures present in each of the images. In general, the degree of similarity between the images is measured from the mutual information (MI) given by equations (1)–(3) [18].

$$MI(A,B) = H(A) + H(B) - H(A|B) \tag{1}$$

$$H(X) = \sum_i P_x \, log_2 P_x \tag{2}$$

$$H(X,Y) = \sum_{x,y} P_{xy} \, log_2 P_{xy} \tag{3}$$

Here, $H(A)$ represents the Shannon entropy relative to the image matrix A, $H(B)$ represents the Shannon entropy relative to the image matrix B. $H(A|B)$ represents the joint entropy, it measures the amount of information contained in image A when image B is known, P_x and P_y are the marginal probabilities, P_{xy} is the joint probability function.

It has been shown that the mutual information measure is sensitive to the amount of overlap between images. Therefore, normalized mutual information was introduced to mitigate this problem. An example of the $NMI(A,B)$ normalized mutual information is given by equation (4) [19].

$$NMI(A,B) = \frac{H(A) + H(B)}{H(A|B)} \tag{4}$$

2.2. About hypothesis testing

The Kolmogorov-Smirnoff *KS* test was first introduced by Kolmogorov [20,21] and Smirnoff [22]. It compares a distribution of theoretical data with that of an empirical distribution that would be expected if the data were normal. Its simplest form is given by equation (5) [23].

$$KS_n = \sqrt{n} Sup_x |F_n(x) - F(x)| \tag{5}$$

The function $F(x)$ is associated with the value of the theoretical distribution in x, and $F_n(x)$ is associated with the value of the empirical distribution for a sample of size n. The value of KS_n is decisive for the conclusion on the hypothesis. If KS_n is greater than the critical value KS_α for a given α, the null hypothesis that $F_n(x)$ comes from the underlying distribution $F(x)$ is rejected. See Massey [24] for critical values for different sample sizes. The two-sample version of the KS test generalizes to equation (6) [23].

$$KS_{nn'} = \sqrt{\frac{nn'}{n+n'}} Sup_x |F_n(x) - F_{n'}(x)| \tag{6}$$

Where $F_n(x)$ and $F_{n'}(x)$ are empirical cumulative distribution functions at time x, and from data of size n and n' respectively. If KS_n is greater than the critical value KS_α for a given α, the null hypothesis that $F_n(x)$ comes from the underlying distribution $F_{n'}(x)$ is rejected. The *KS* test is very sensitive to the shape of a distribution. Indeed, it can detect differences everywhere along the scale which makes it mainly advantageous. The other advantage is that it is suitable for experimental situations with a small number of samples [23].

The Anderson-Darling test was originally developed to solve problems in the field of engineering. It was developed in 1952 by T W. Anderson and D.A. Darling [25] as an alternative to other statistical methods. The objective is to detect deviations from normality of sample distributions. This test is characterised by its non-directionality. For one sample tests and is given by equation (7) [23].

$$AD = -n - \frac{1}{n}\sum_{i=1}^{n}(2i-1)\left[\ln\left(x_{(i)}\right) + \ln\left(1 - \left(x_{(n+1-i)}\right)\right)\right] \tag{7}$$

Where $\{x(1) < \ldots x(n)\}$ is the sample of size n arranged in ascending order, and $F(x)$ is the underlying theoretical cumulative distribution against which the sample is compared. If *AD* is greater than the critical value AD_α for a given α, the null hypothesis that $\{x(1) < \ldots x(n)\}$ comes from the underlying distribution F(x) is rejected. There is also the two-sample *AD* test, introduced by Darling [26] and Pettitt [27], which generalizes according to equation (8).

$$AD = \frac{1}{mn}\sum_{i=1}^{n+m}\left(N_i Z_{(n+m-ni)}\right)^2 \frac{1}{iZ_{(n+m-i)}} \tag{8}$$

$Z(n+m)$ is the ordered combination of the data $X(n)$ and $Y(m)$, of size n and m, and Ni is the number of observations in $Z(n)$ that are equal to or less than the ith observation in $Z(n+m)$. The null hypothesis that the data $X(n)$ and $Y(m)$ are from the same distribution is rejected if *AD* is greater than the corresponding critical value.

The Shapiro-Wilk test tests the null hypothesis that a sample $x_1 \ldots x_n$ comes from a normally distributed population. It is defined according to equation (9) [23].

$$W = \frac{\left(\sum_{i=1}^{n} a_i x_{(i)}\right)^2}{\sum_{i=1}^{n}\left(x_i - \bar{x}\right)^2} \tag{9}$$

With $x(i)$ the i-th order statistic, i.e. the i-th smallest number in the sample. The constants a_i are given by equation (10) [23].

$$(a_1, \ldots, a_i) = \frac{m^\top V^{-1}}{\left(m^\top V^{-1} V^{-1} m\right)^{1/2}} \tag{10}$$

Where $m = (m_1, \ldots m_n)^\top$ and $m_1, \ldots m_n$ are the expected values of the order statistics of independent and identically distributed random variables sampled from the standard normal distribution, and V is the covariance matrix of those order statistics.

In the end, the normality of the data observed from the different statistics mentioned, are verified from the p-value. The p-value is used to quantify the statistical significance of a result in the case of a null hypothesis. The objective is to determine whether the null hypothesis is verified or not. If it is, the observed result is highly unlikely. This is an extension of the principle of proof by the absurd. As it is a probability value, the p-value is calculated as a value between zero and one.

3. Experimental details

3.1. Experimental set-up

The experimental set-up consists of a Marx generator (200 kV - 1.25 kJ) which provides a standard negative and positive lightning impulse voltage (1.2/50 μs), a control case, a capacitive voltage divider, a shunt current sensor. All this equipment developed in

Cameroon is the property of the University Institute of Technology of the University of Douala in Cameroon. The test cell is a porcelain vessel with a volume of 5 L and a wall thickness of 10 mm. It is entirely covered with transparent glass of 8 mm thickness. It contains a tungsten tip electrode with a tip radius of 50 μm. The tip is a product of the Zhuzhou Hongtong Tungsten Carbide Co in China. The flat brass electrode with a thickness of 30 mm and a diameter of 250 mm was machined on site in Cameroon. The volume of oil used for each test is 3 L. The pressboard used is 10 mm thick, with a square shape of 120 mm per side. The optical discharge detection system consists of a Panasonic GP-KR22 CCD colour camera and a computer. Fig. 1 shows the schematic diagram used for the measurement. The images and data are processed using OriginPro and Matlab software.

3.2. Esters processing

The biobased insulating liquid is obtained from dried palm nuts. The vegetable oil is extracted from the nuts by mechanical pressure using an auger after the nuts have been crushed. The liquid obtained is then decanted for 48 h. This stage is followed by a degumming operation. This consists of extracting the phospholipids and gums that may become insoluble through hydration. To do this, demineralised water heated to 90 °C is added to the oil in a proportion of 20%. The whole is mixed slowly at 30 rpm for 40 min with the help of a stirrer. After decanting, the oil is separated from the gums and can be recovered. The next step is to add sodium hydroxide (NaOH) to the oil, at a concentration of 14°Be. This stage of the process reduces the acid number by neutralising the free fatty acids. The last step consists of reducing the viscosity of the liquid resulting from transesterification [28]. Indeed, at room temperature, vegetable oils are generally subject to rancidity and crystallisation. Adding a basic catalyst such as potassium hydroxide (KOH) to the liquid allows it to be separated from the glycerol which is the main cause. The esters obtained are finally dried at 80 °C for 24 h [29,30].

3.3. Extraction of mutual information

Finding the ideal transformation matrix for image registration usually requires knowledge of at least eight twin points. However, images of creeping discharges are almost random in nature. Therefore, we propose a method based on a random search of similarity points. The search is performed by extracting the maximum mutual information. The method consists of extracting the binary image from the real image. The binary image is then skeletonised. Of the two images to be compared, one image is kept fixed. From the centre of the second image, progressive translations and rotations of the second image around the first image are performed, while searching for the mutual information. The mutual information data and the different translation and rotation operations are stored in matrices. By plotting the information surface, it becomes easy to determine the geometric transformation parameters for the special matching of the two images to provide an objective discussion. If we call N the number of images obtained in each insulating liquid for the same voltage level, the final information NMI is the average of the information of N^2 image permutations as presented by equations (11) and (12). With i and j the indices of the different permutations of images X and Y in the calculation of the information. Fig. 2 shows the complete flowchart of the maximum information extraction method.

$$NMI = \frac{1}{N^2} \sum_{i=1,j=1}^{N} NMI(X_i, Y_j) \tag{11}$$

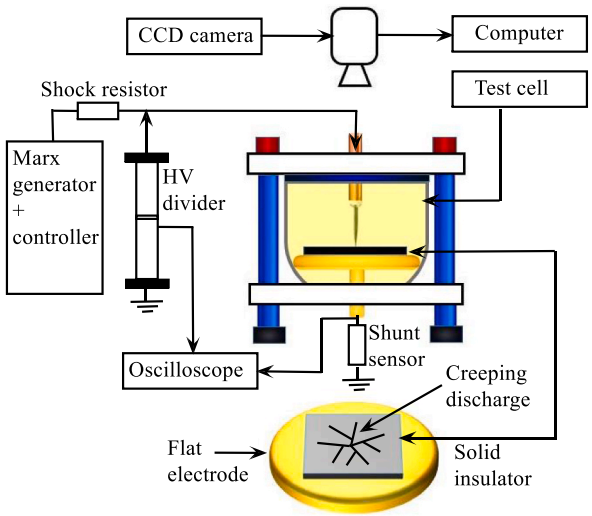

Fig. 1. Experimental set-up.

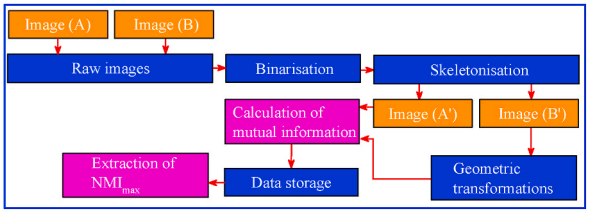

Fig. 2. Algorithm for extracting information.

$$NMI = \frac{1}{N^2}\sum_{i=1,j=1}^{N}\left(\frac{H(X_i)+H(Y_j)}{H(X_i,Y_j)}\right) \tag{12}$$

3.4. Calculation of the discharge extension

The maximum length of the discharge is taken as the distance from the tip to the end of the longest branch of the discharge. An illustrative description of the length calculation process is detailed in a previous articles [31,32]. Similarly, the total length of the discharges is obtained after binarisation of the original image. The technique consists of counting the number of pixels in the image obtained after binarisation and skeletonisation, and then multiplying the result by a coefficient related to the camera position. The value of the coefficient is obtained by initially filming an image of known size to determine the millimetre equivalent of a pixel. Fig. 3a and b shows an example of a discharge image obtained after skeletonisation.

3.5. Determination of the fractal parameter

In this work, the calculation of the fractal parameter is performed using the box-counting technique commonly used in this situation [6]. The process consists first of the binarisation of the original image. Thereafter, the output image is entirely covered with a number N of square boxes of size r (unit in pixels). The fractal dimension is obtained by determining the slope of the plot of the log-log function of N versus r as we vary the size of the boxes. Equations (13) and (14) give the relationships between the fractal parameter (D), the number of boxes (N) and the box size r.

$$N(r) \sim r^{-D} \tag{13}$$

$$D = -\lim_{r\to 0}\frac{logN(r)}{\log\,(r)} \tag{14}$$

4. Results and discussion

4.1. Analysis of the shape of discharges

The visual examination of the discharges presented in Fig. 4a to d at ¼ scale and obtained in MO and PKOME shows that they have a filamentary aspect as reported by Kebbabi et al. in Ref. [5]. However, they have a more or less radial shape contrary to the results reported in Refs. [6,33]. This result shows that apart from the type of solid/liquid isolation system used, the experimental setup has an impact on the way discharges propagate. The images obtained also show a significant ionisation phenomenon around the tip, independent of the nature of the insulating liquid. This result can be justified by the fact that the distribution of the electric field is inhomogeneous due to the experimental configuration of the tip and plane of the electrodes. Such a configuration favours the intensification of the field at the tip as demonstrated by Beroual et al. in Ref. [6]. This result was also confirmed by electric field

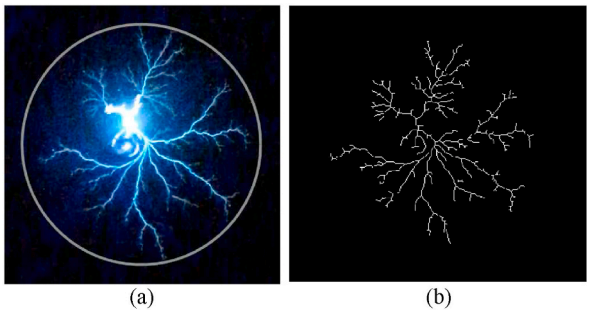

Fig. 3. Illustration of the method for calculating the length of discharge; (a): original image, (b): Skeleton.

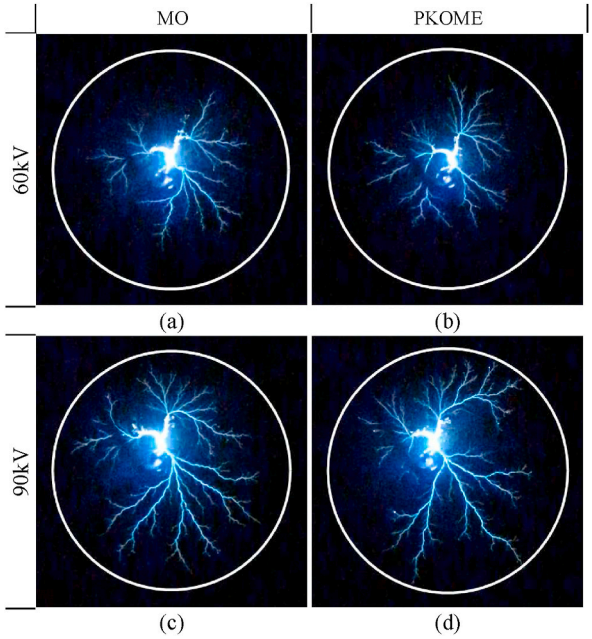

Fig. 4. Discharges obtained in the MO (a, b) and PKOME (b, d) under negative lightning pulse voltage.

simulations as shown in Fig. 5a and b, carried out on pressboard immersed in mineral oil in point-plane geometry. The simulation is done on COMSOL Multiphysics software and based on the finite element method. It was concluded that the electric field distribution at the point is more intense than on the rest of the insulating surface. On the other hand, we also notice that the increase of the amplitude of the applied voltage has the effect of increasing the maximum extension of the discharges. The behaviour is the same for the degree of branching of discharges. A similar result is reported in Ref. [4]. This result is to be expected, as increasing the applied voltage intensifies the electric field on the insulating structure. The intensification of the field on the insulating structure leads to polarisation of the structure, resulting in capacitive effects. The charge density at the surface of the solid insulator and the charge carrier displacement field are related to the electric field present. This relationship leads to an increase in the mobility of the charge carriers. This phenomenon is verified by the equations governing solid insulation given by Gauss's law, as shown in equations 15–17 [34].

$$-\nabla.(\varepsilon\nabla V) = 0 \tag{15}$$

$$\nabla.J_{SD} = 0 \tag{16}$$

$$\frac{\partial T}{\partial t} = \frac{1}{\rho_{SD}C_{SD}}\left(k_{SD}\nabla^2 T\right) \tag{17}$$

Where the current density J_{SD} is zero because the solid insulator has zero conductivity. ρ_{SD} is the mass density, C_{SD} is the specific heat capacity, and k_{SD} is the thermal conductivity in the solid insulator region.

The surface charge density, σ_s at the liquid-solid dielectric interface can be calculated as shown in equation (18).

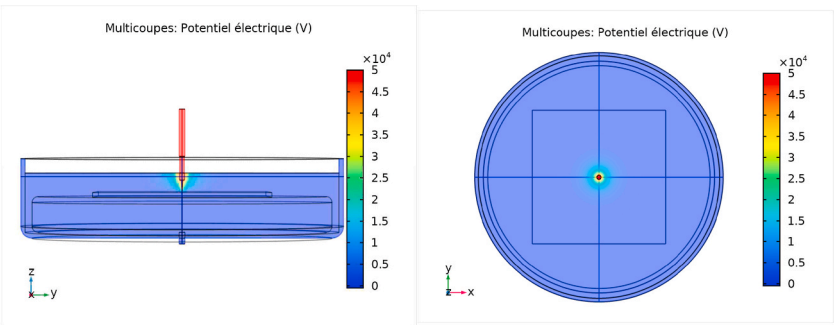

Fig. 5. Example of electrical potential distribution on pressboard immersed in PKOME.

$$\frac{\partial \sigma_s}{\partial t} = n.(J_+ + J_- + J_e) \tag{18}$$

Where $J_i = \rho_i \mu_i E$, and n is the unit vector of the exterior normal of the solid to the liquid. The surface charge density can be calculated using Gauss' law as given by equations (19) and (20) [34].

$$\sigma_s = n.\left(D_{solid} - D_{liquid}\right) \tag{19}$$

Where $D = \varepsilon_r E$ (20)

D represents the electric charge distribution in the insulating medium under study in response to the presence of an applied electric field E.

4.2. Impact of relaxation time on fractal dimension

The behaviour of the fractal parameter of the discharges was analyzed by two methods. The first method is based on the observation of the variation of this parameter as a function of the relaxation time of the liquids. The results of the experiment presented in Fig. 6 show that, independently of the nature of the insulating liquid used, very short relaxation times lead to a strong instability of the fractal dimension. A progressive increase of the relaxation time leads to a convergence of the fractal dimension. We also notice that, for results taken under the same experimental conditions, the stabilisation time of the fractal dimension is shorter in PKOME than in MO. This result can be justified by the physicochemical parameters of the insulating liquids. Indeed, the distribution of the space charge density on an immersed solid surface corresponds to the distribution of a decreasing exponential function whose argument depends on the relaxation time of the liquid used. The relaxation time of the space charges corresponds to the ratio of the permittivity of the liquid to its thermal conductivity. On the other hand, it is known that the thermal conductivity of PKOME is higher than that of MO and of smaller value than one, so this implies a longer relaxation time with MO. This result shows on the one hand that, during laboratory experiments, the physicochemical characteristics of the insulators used must be taken into consideration when deciding on the relaxation time to be given to each liquid before the experiments are resumed, in order to avoid as much measurement error as possible. On the other hand, the convergence towards an almost fixed value of the fractal dimension with the long relaxation times shows that the generation and propagation of this type of discharge is not a totally random phenomenon but strongly depends on the physicochemical properties of the insulation system. It is noted that the fractal dimension increases as the permittivity of the insulating liquid decreases, a similar result is reported in Ref. [35].

The second method of analysis is based on hypothesis testing. Fractal dimension data analyzed from the Anderson Darling test, the Kolmogorov-Smirnov test and the Shapiro-Wilk test show that space charges and capacitive effects caused by very short relaxation times have the effect of producing results that deviate from the normal law. Table 1 presents a summary of the results of the hypothesis tests obtained for the three statistics as a function of relaxation time.

Such a result implies that the generation and propagation of discharges could be unpredictable and therefore uncontrollable phenomena. On the other hand, long relaxation times lead to an almost complete alignment of the fractal dimension data with the regression line of the normal law as shown in Fig. 7a to f for the Anderson Darling test.

This result therefore presents an inverse effect and indicates that the relaxation time has a direct impact on the measurements during the experiment. This is confirmed by the validation of the null hypothesis through the increase of the p-value and the decrease of the Anderson Darling (AD) coefficient, for relatively long times as represented in Fig. 8. The same analysis applied to the evaluation of the maximum extension of the discharges as a function of the relaxation. Fig. 9 shows the variation of ten values of maximum discharge extension as a function of relaxation time and for a fixed voltage of 70 kV. The results show that very short relaxation times amplify the measurement error and increase the maximum extension of the discharge. In practice, all these results show that in the case

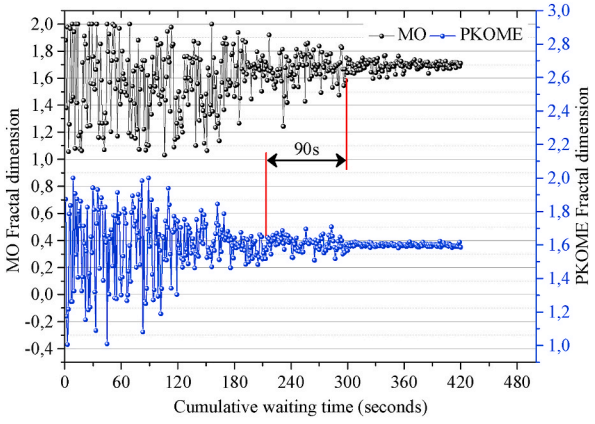

Fig. 6. Evolution of the fractal dimension in MO and PKOME as a function of relaxation time.

Table 1
Conformity test as a function of relaxation time.

Waiting time (s)	ANDERSON-DARLING			KOLMOGOROV-SMIRNOV			SHAPIRO-WILK		
	AD	*P*-value	Conformity	KS	*P*-value	Conformity	W	*P*-value	Conformity
60	0.784	0.027	No	0.315	0.010	No	0.929	0.083	No
120	0.721	0.040	No	0.284	0.030	No	0.926	0.074	No
180	0.627	0.072	Yes	0.223	0.126	Yes	0.940	>0.100	Yes
240	0.348	0.398	Yes	0.217	>0.150	Yes	0.960	>0.100	Yes
300	0.245	0.683	Yes	0.148	>0.150	Yes	0.981	>0.100	Yes
360	0.217	0.783	Yes	0.138	>0.150	Yes	0.980	>0.100	Yes
420	0.205	0.821	Yes	0.139	>0.150	Yes	0.986	>0.100	Yes

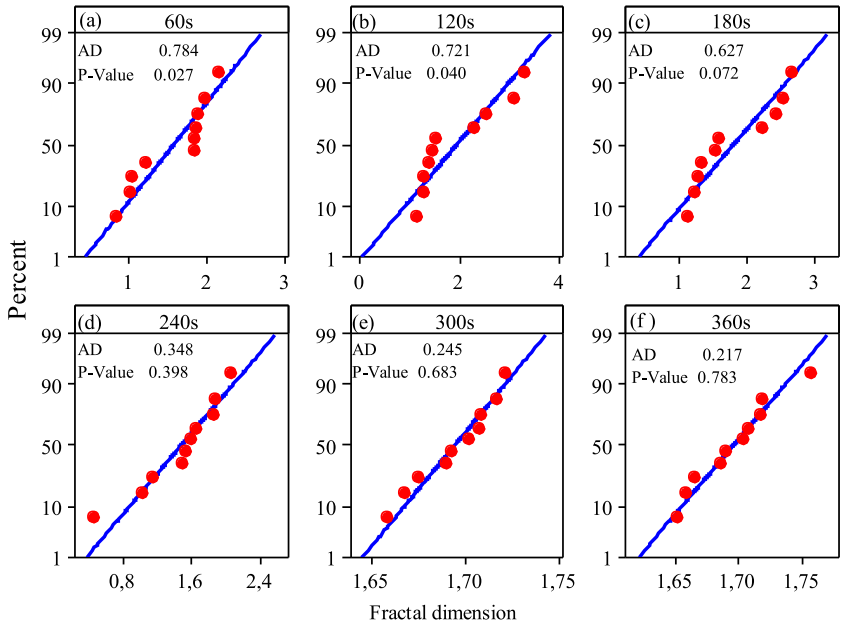

Fig. 7. Distribution of fractal dimension data as a function of relaxation time for the Anderson Darling test.

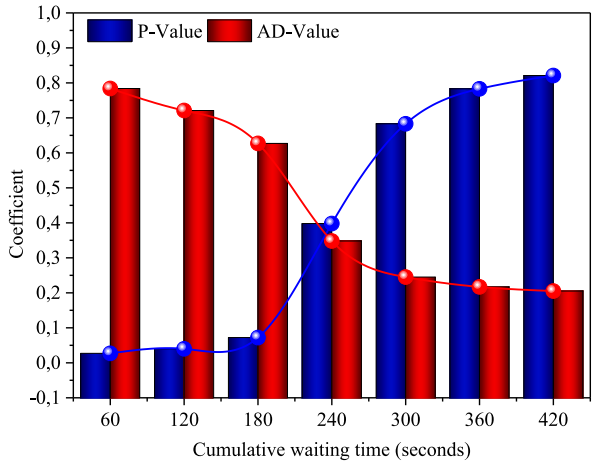

Fig. 8. Evolution of *P*-Value and AD-Value in MO as a function of relaxation time.

of a real transformer, the impact of such a phenomenon on the insulating surface can be predicted when it appears at long time intervals. When the phenomenon starts to occur at very short time intervals, there is a greater risk of chaotic behaviour and damage to the insulation system.

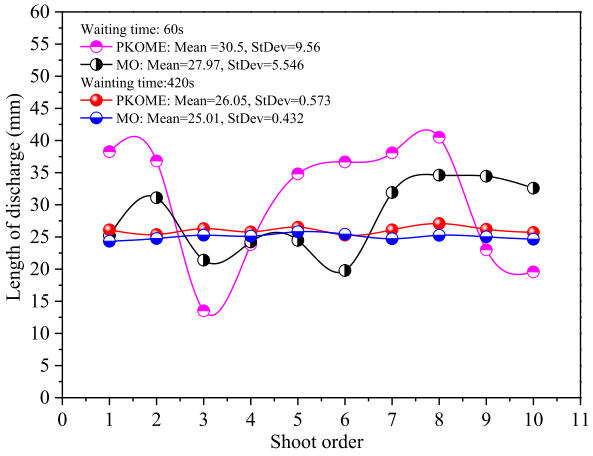

Fig. 9. Maximum extension of discharges as a function of relaxation time.

4.3. Impact of relaxation time on mutual information

When two images or two systems share the same information, the mutual information surface has a single peak whose maximum is 100%. Fig. 10a shows an example of the resulting information surface obtained when comparing an image with itself. It can be seen that there is no need for a geometrical transformation to obtain such a result as shown in the figure, because the algorithm takes into account the position of each pixel in the image. The same method applied to images obtained in MO and PKOME under the same experimental conditions with a relatively short relaxation time of 60s shows that the images do not share information. Several peaks are observed with a maximum of 4% as shown in the example in Fig. 10b. However, a longer relaxation time of 240s has the effect of reducing the number of peaks on the information surface. An average increase in the amplitude of the information maximum to 45% is observed as shown in the example in Fig. 10c. A relaxation time of 420s concentrates all the information in a single peak as in the case of mutual information between an image and itself, with an increase in amplitude to 60% as shown in the example in Fig. 10d. In general, it can be seen that with the increased relaxation times, discharges that initially did not share information start to have similarities. The same comparison made with images obtained at different voltage levels shows a maximum of almost no information. These results indicate that the phenomenon is not totally random with high relaxation times.

4.4. Implication of mutual information and extension of discharges in the characterisation of MO and PKOME

It is important to note that the mutual information parameter is very important in the characterisation of discharges from a comparative point of view. Indeed, the mutual information takes into account the morphology of the discharges through the geometrical position of each pixel of the images to be compared. This implies that, if an image is denser, more branched or has a totally different morphology from another, then the mutual information will be almost null. The first method of comparing the discharges obtained in MO and PKOME was based on extracting the maximum information through the analysis of the mutual information surface. The output data shows that the plot of the maximum information as a function of the relaxation time follows the evolution of a logistic function with a regression coefficient of 99% as presented in Fig. 11. We also notice that the information curves returned by the images from the MO/MO, PKOME/PKOME and MO/PKOME systems are almost identical at 60% for a cumulative relaxation time of 420s. The result for the MO/PKOME system is almost the same as that for the MO/MO system, which leads to the conclusion that the discharge propagation is almost the same in both liquids.

The second approach is based on the calculation of the maximum extension and the total length of the discharges as found in the literature. This technique allows to see on the one hand a linear evolution of the discharge extension with the applied voltage as shown in Fig. 12a and b. On the other hand, it can be seen that the maximum extension and the total length of the discharges is 4% identical in the two liquids. This difference explains the fact that the maximum mutual information does not exceed 60%. This result is promising for PKOME, which is positioned as a potential substitute for MO in case of future depletion of sickle resources. Indeed, previous work on the propagation of creeping discharges on pressboard immersed in vegetable oils compared to those produced in mineral oil has shown quite different results. Among these, we note the work of Beroual et al. [6] on the analysis of these creeping discharges should be noted. In a comparative study of the ability of mineral oils (MO) and vegetable oils to dampen the propagation of these discharges, they show that for positive voltage stresses, the lengths of the branches are 60% higher in vegetable oils than in MO. This result is revised to 40% at a negative voltage under the same conditions. The vegetable oils studied in this work are, among others, vegetable oils extracted from grape seed (GS), sunflower (SF) and rapeseed (RS). An almost similar result is shown by Sitorus et al. [4]. For similar analyses conducted in the case of Jatropha curcas methyl ester (JMEO). They show that the level of attenuation of the discharge spread is 60% higher for MO than for vegetable oil. Reffas et al. [7] carried out the same investigations. The insulating liquids used were extra virgin olive oil (OO) without additives, synthetic esters of methyl oleate (MY) and tetra-ester (SE), a natural ester of rapeseed oil (RO) and mineral oil of naphthenic nature (MO). In their work, graphical representations of the maximum length of the discharges as a

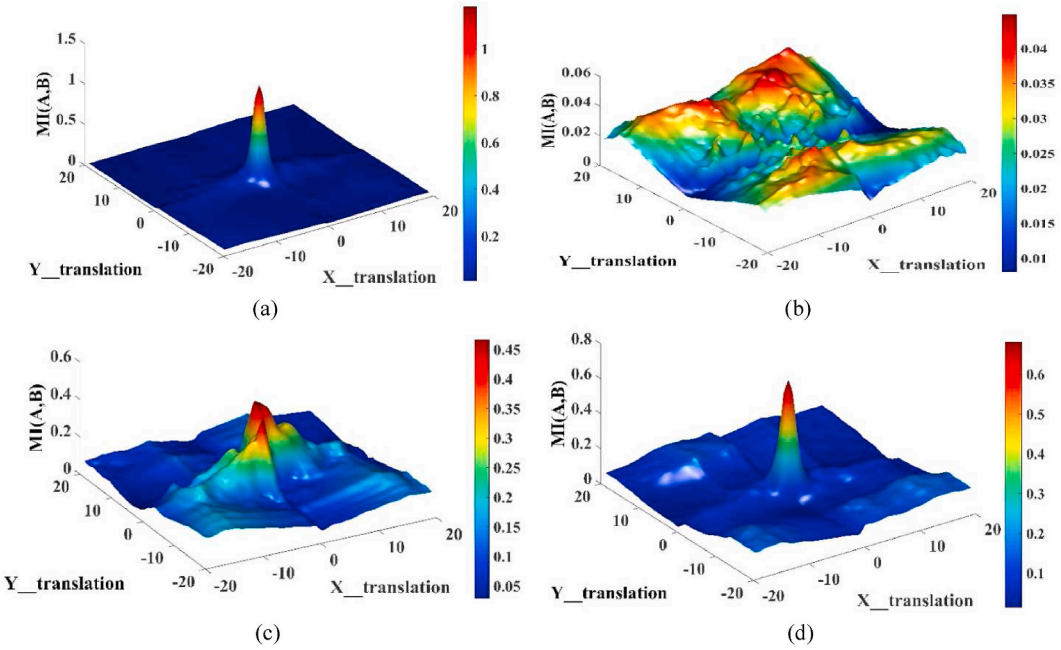

Fig. 10. Information surface between: (a): an image and itself; (b, c, d): Information surfaces between ten images obtained with relaxation times of 60s, 240s and 420s respectively.

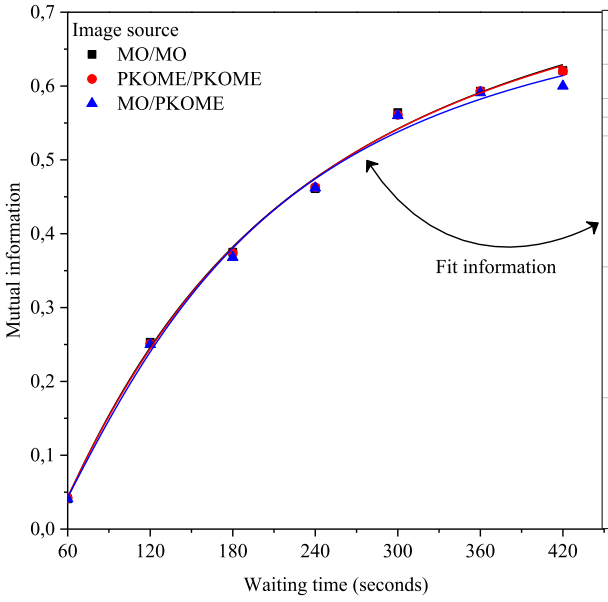

Model	Logistic		
Equation	y = A2 + (A1-A2)/(1 + (x/x0)^p)		
Reduced Chi-Sqr	2,86318E-4	2,27226E-4	3,94685E-4
Adj. R-Square	0,99355	0,99486	0,99081
		Value	Standard Error
MO/MO	A1	-0,21555	0,27044
	A2	0,8672	0,2442
	x0	152,32811	26,73471
	p	1,24804	0,70216
	EC20	50,1621	34,87713
	EC50	152,32811	26,73471
	EC80	462,57738	277,2598
PKOME/PKOME	A1	-0,18918	0,20526
	A2	0,84707	0,1905
	x0	154,30907	21,73927
	p	1,31339	0,60372
	EC20	53,70188	28,65109
	EC50	154,30907	21,73927
	EC80	443,39771	210,72202
MO/PKOME	A1	-0,12518	0,16866
	A2	0,75893	0,14432
	x0	149,87742	21,46916
	p	1,58288	0,72272
	EC20	62,4279	29,14742
	EC50	149,87742	21,46916
	EC80	359,82693	136,00119

Fig. 11. Evolution of mutual information as a function of relaxation time.

function of the applied voltage are shown. The analysis of their results shows that the mineral oil has a greater ability to stop the propagation of discharges. Ediriweera et al. [36] conducted this investigation for discharges propagating on glass immersed in vegetable oils. The oils studied include natural esters such as: coconut oil copra type, virgin coconut oil, soybean oil and sunflower oil. Their results were compared with those of Kebbabi et al. [37] for discharges propagating on glass immersed in mineral oil. The analysis showed that mineral oil was more effective in stopping the propagation of discharges.

5. Conclusion

The objectives of this work were to study the impact of the relaxation time of insulating liquids on the characteristic parameters of

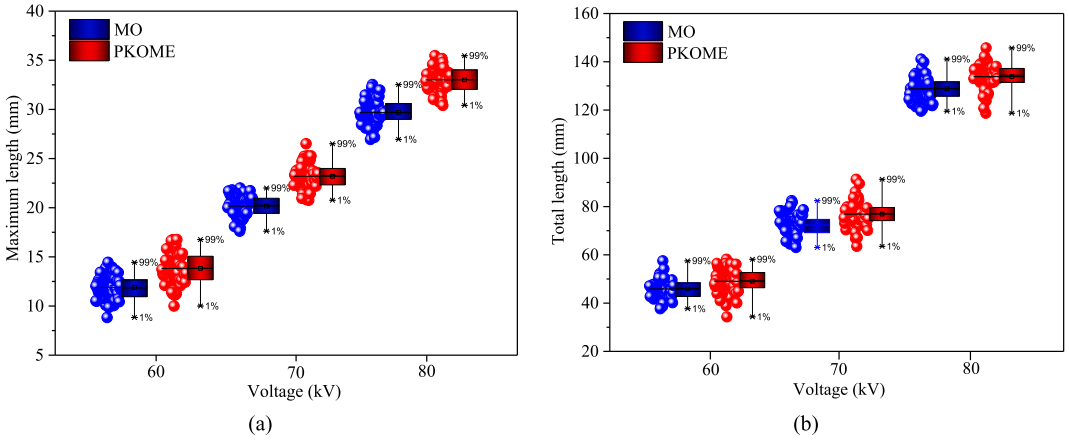

Fig. 12. Evolution of the maximum (a) and total (b) length of discharges as a function of the applied voltage.

creeping discharges. In addition, a comparative study of creeping discharges propagating on pressboard immersed in palm kernel oil methyl ester (PKOME) compared to those produced in mineral oil (MO). Based on the algorithms for calculating the mutual information, the algorithms for calculating the maximum and total extension of the discharges, the low-level analyses of the normality hypothesis test through the Anderson-Darling, Kolmogorov-Smirnov and Shapiro-Wilk statics, we have shown that:

- The very short relaxation times maintain the capacitive effects and increase the measurement error, which leads to a disorderly variation of the characteristic parameters such as: fractal dimension, maximum extension and total length of the discharges.
- The relaxation time of each liquid is strongly related to its physicochemical characteristics. It decreases as the thermal conductivity of the liquid increases.
- Tests of the normality hypothesis showed that for large relaxation times, fractal-sized data follow the normal distribution.
- The analysis of the mutual information surface led to the conclusion that, for relatively large relaxation times, the discharge propagation phenomenon is not totally random.
- The analysis of the mutual information and the total length of the discharge images from palm kernel oil methyl ester and mineral oil showed that the propagation is almost identical in both liquids.

Combining the information obtained from these experiments with other investigations presented in the literature, it can be said that palm kernel oil methyl ester is positioned as a potential substitute for mineral oils in the case of the depletion of sickle resources in the future.

Declarations

Author contribution statement

Jean Lambert Jiosseu: Conceived and designed the experiments; Performed the experiments; Analyzed and interpreted; Contributed reagents, materials, analysis tools or data; Wrote the paper.

Ghislain Mengata Mengounou: Conceived and designed the experiments; Performed the experiments; Analyzed and interpreted; Contributed reagents, materials, analysis tools or data.

Emeric Tchamdjio Nkouetcha: Conceived and designed the experiments; Performed the experiments; Analyzed and interpreted; Contributed reagents, materials, analysis tools or data.

Adolphe Moukengue Imano: Conceived and designed the experiments; Performed the experiments; Analyzed and interpreted; Contributed reagents, materials, analysis tools or data.

Funding statement

The authors of this paper did not receive any specific grant from funding agencies in the public, commercial, or not-for-profit sectors.

Data availability

The data used to write this paper is confidential.

Additional information

No additional information is available for this paper.

Declaration of competing interest

The authors declare that they have no known competing financial interests or personal relationships that could have appeared to influence the work reported in this paper.

References

[1] P. Rozga, A. Beroual, High Voltage Insulating Materials—Current State and Prospects, 2021, p. 3799, https://doi.org/10.3390/en14133799, vol. 14, no. 13, ed: MDPI.
[2] Yuan Li, Yahong Li, J. Wen, L. Li, L. Wang, G. Zhang, How cellulose particles influence streamer propagation and branching in transformer oil: a 2D modelling perspective, Plasma Res. Exp. 2 (2) (2020), 025011, https://doi.org/10.1088/2516-1067/ab9539.
[3] B. Qi, Z. Wei, C. Li, Creepage discharge of oil-pressboard Insulation in AC-DC composite field: phenomenon and characteristics, IEEE Transact. Dielectr. 23 (1) (2016) 237–245, https://doi.org/10.1109/TDEI.2015.005404.
[4] H.B. Sitorus, A. Beroual, R. Setiabudy, S. Bismo, Creeping discharges over pressboard immersed in jatropha curcas methyl ester and mineral oils, in: 2015 IEEE 11th International Conference on the Properties and Applications of Dielectric Materials (ICPADM), IEEE, 2015, pp. 152–155, https://doi.org/10.1109/ICPADM.2015.7295231.
[5] L. Kebbabi, A. Beroual, Optical and electrical characterization of creeping discharges over solid/liquid interfaces under lightning impulse voltage, IEEE Transact. Dielectr. 13 (3) (2006) 565–571, https://doi.org/10.1109/TDEI.2006.1657969.
[6] A. Beroual, V.-H. Dang, Fractal analysis of lightning impulse surface discharges propagating over pressboard immersed in mineral and vegetable oils, IEEE Transact. Dielectr. 20 (4) (2013) 1402–1408, https://doi.org/10.1109/TDEI.2013.6571462.
[7] A. Reffas, A. Beroual, H. Moulai, Comparison of creeping discharges propagating over pressboard immersed in olive oil, mineral oil and other natural and synthetic ester liquids under DC voltage, IEEE Transact. Dielectr. 26 (6) (2019), https://doi.org/10.1109/TDEI.2019.008313.
[8] S. Ediriweera, P. Jayarathna, R. Samarasinghe, R. Lucas, Investigation on the effect of the cross-section of insulators on the radial discharge distribution of creeping discharges, in: 2021 IEEE International Conference on the Properties and Applications of Dielectric Materials (ICPADM), IEEE, 2021, pp. 159–162, https://doi.org/10.1109/ICPADM49635.2021.9493995.
[9] M. Huang, et al., Effect of nanoparticle shapes on creeping flashover characteristics at the interface of nanofluid-impregnated pressboard, IEEE Transact. Dielectr. 25 (3) (2018) 1135–1141, https://doi.org/10.1109/TDEI.2018.007058.
[10] G. Haskins, U. Kruger, P. Yan, Deep learning in medical image registration: a survey, Mach. Vis. 31 (8) (2020) 1–18, https://doi.org/10.1007/s00138-020-01060-x.
[11] M. Pan, F. Zhang, Medical image registration based on Renyi's quadratic mutual information, IETE J. Res. 68 (6) (2022) 4100–4108, https://doi.org/10.1080/03772063.2020.1787873.
[12] L. Tang, Y. Deng, Y. Ma, J. Huang, J. Ma, SuperFusion: a versatile image registration and fusion network with semantic awareness, IEEE/CAA J. Automat. Sinica 9 (12) (2022) 2121–2137, https://doi.org/10.1109/JAS.2022.106082.
[13] D. Sengupta, P. Gupta, A. Biswas, A survey on mutual information based medical image registration algorithms, Neurocomputing 486 (2022) 174–188, https://doi.org/10.1016/j.neucom.2021.11.023. C.
[14] J.P. Pluim, J.A. Maintz, M.A. Viergever, Interpolation artefacts in mutual information-based image registration, Comp. Vis. 77 (2) (2000) 211–232, https://doi.org/10.1006/cviu.1999.0816.
[15] J.P. Pluim, J.A. Maintz, M.A. Viergever, Mutual-information-based registration of medical images: a survey, IEEE Trans. Med. Imag. 22 (8) (2003) 986–1004, https://doi.org/10.1109/TMI.2003.815867.
[16] J.P. Pluim, J.B.A. Maintz, M.A. Viergever, Image registration by maximization of combined mutual information and gradient information, in: Medical Image Computing and Computer-Assisted Intervention–MICCAI 2000: Third International Conference, Pittsburgh, PA, USA, October 11-14, 2000. Proceedings 3, Springer, 2000, pp. 452–461, https://doi.org/10.1007/b12345.
[17] E. Haber, J. Modersitzki, Beyond mutual information: a simple and robust alternative, in: Bildverarbeitung für die Medizin 2005: Algorithmen—Systeme—Anwendungen Proceedings des Workshops vom 13.–15. März 2005 in Heidelberg, Springer, 2005, pp. 350–354, https://doi.org/10.1007/3-540-26431-0_72.
[18] J. Wang, X. Dai, H. Luo, C. Yan, G. Zhang, J. Luo, MI_DenseNetCAM: a novel pan-cancer classification and prediction method based on mutual information and deep learning model, Front. Genet. 12 (2021), 670232, https://doi.org/10.3389/fgene.2021.670232.
[19] R. Koopman, S. Wang, Mutual information based labelling and comparing clusters, Scientometrics 111 (2) (2017) 1157–1167, https://doi.org/10.1007/s11192-017-2305-2.
[20] A. Kolmogorov, Sulla determinazione empirica di una legge didistribuzione, Giorn Dell'inst Ital Degli Att 4 (1933) 89–91, 101111/j.1741-4520.2006.00116.x.
[21] A. Kolmogoroff, Confidence limits for an unknown distribution function, Ann. Math. Stat. 12 (4) (1941) 461–463. https://www.jstor.org/stable/2235958.
[22] N. Smirnoff, Sur les écarts de la courbe de distribution empirique, Matematicheskii Sbornik 48 (1) (1939) 3–26. https://www.mathnet.ru/eng/sm/v48/i1/p3.
[23] S. Engmann, D.J. Cousineau, Comparing distributions: the two-sample Anderson-Darling test as an alternative to the Kolmogorov-Smirnoff test, J. Appl. Quant. Methods 6 (3) (2011).
[24] J. Frank, Massey Jr., The Kolmogorov-Smirnov test for goodness of fit, J. Am. Stat. Assoc. 46 (253) (1951) 68–78, https://doi.org/10.1080/01621459.1951.10500769.
[25] T.W. Anderson, D.A. Darling, Asymptotic theory of certain" goodness of fit" criteria based on stochastic processes, Ann. Math. Stat. 23 (No. 2) (1952) 193–212, https://doi.org/10.1214/aoms/1177729437.
[26] D.A. Darling, The Kolmogorov-smirnov, cramer-von mises tests, Ann. Math. Stat. 28 (4) (1957) 823–838. https://www.jstor.org/stable/2237048.
[27] A. Pettitt, A two-sample Anderson-Darling rank statistic, Biometrika 63 (1) (1976) 161–168, https://doi.org/10.1093/biomet/63.1.161.
[28] A. Abdelmalik, J. Fothergill, S. Dodd, Aging of Kraft paper insulation in natural ester dielectric fluid, in: 2013 IEEE International Conference on Solid Dielectrics (ICSD), IEEE, 2013, pp. 541–544, https://doi.org/10.1109/ICSD.2013.6619678.
[29] E.T. Nkouetcha, G.M. Mengounou, A.M. Imano, Elaboration and performance analysis of a bio-based insulating liquid from castor oil for power transformers, Open Acc. Libr. J. 6 (5) (2019) 1, https://doi.org/10.4236/oalib.1105404.
[30] S. Ravulapalli, R. Kunta, M.J. Ramamoorty, Preparation, characterization and feasibility analysis of methyl ester of Sesbania seeds oil (MESSO) as alternate liquid dielectrics in distribution transformers, RSC Adv. 9 (6) (2019) 3311–3319, https://doi.org/10.1039/C8RA08378A.
[31] J.L. Jiosseu, G.M. Mengounou, A.M. Imano, Study of creeping discharges propagating along a solid insulating surface immersed in mineral oil and palm kernel oil methyl ester under negative lightning impulse voltage, IEEE Transact. Dielectr. 29 (5) (2022) 1847–1856, https://doi.org/10.1109/TDEI.2022.3199183.
[32] J.L. Jiosseu, G.M. Mengounou, A.M. Imano, Experimental characterisation of positive creeping discharges propagating along an insulating surface immersed in vegetable and mineral oil, J. Electrost. 119 (2022), 103753, https://doi.org/10.1016/j.elstat.2022.103753.

[33] A. Beroual, Relationship between the physicochemical properties of materials and the fractal dimension of creeping discharges propagating at solid/fluid interfaces, in: 2016 IEEE International Power Modulator and High Voltage Conference (IPMHVC), IEEE, 2016, pp. 296–299, https://doi.org/10.1109/IPMHVC.2016.8012899.
[34] N. Liu, J. Zhang, X. Wu, Asset analysis of risk assessment for iec 61850-based power control systems—part i: methodology, IEEE Trans. Power Deliv. 26 (2) (2010) 869–875, https://doi.org/10.1109/TPWRD.2010.2090951.
[35] A. Beroual, M.L. Coulibaly, Fractal analysis of creeping discharge propagating over solid insulators immersed in gases at different pressures, in: 2012 Annual Report Conference on Electrical Insulation and Dielectric Phenomena, IEEE, 2012, pp. 335–338, https://doi.org/10.1109/CEIDP.2012.6378789.
[36] S. Ediriweera, P. Jayarathna, R. Samarasinghe, R. Lucas, Influence of thickness of solid insulators on creeping discharges propagating over epoxy and glass insulators immersed in coconut oil, in: 2020 IEEE Electric Power and Energy Conference (EPEC), IEEE, 2020, pp. 1–6, https://doi.org/10.1109/EPEC48502.2020.9320088.
[37] L. Kebbabi, A. Beroual, Optical and electrical characterization of creeping discharges over solid/liquid interfaces under lightning impulse voltage, IEEE Trans. Dielectr. Electr. Insul. 13 (3) (2006) 565–571, https://doi.org/10.1109/TDEI.2006.1657969.